ACS central science

http://pubs.acs.org/journal/acscii

Research Article

A Molecular Logic Gate for Developing "AND" Logic Probes and the Application in Hepatopathy Differentiation

Mengqi Chen, Chunhong Wang, Zexuan Ding, Hao Wang, Yu Wang, and Zhibo Liu*

Cite This: *ACS Cent. Sci.* 2022, 8, 837−844

Read Online

ACCESS | Metrics & More | Article Recommendations | Supporting Information

ABSTRACT: Accurate diagnosis and therapy are challenging because most diseases lack a single biomarker that distinguishes them from other disorders. A solution would enhance targeting accuracy by using AND-gated combinations of two disease-associated stimuli. Here, we report a novel "AND" molecular logic gate, enabling a double-controlled release of intact functional molecules. Benefiting from a significant difference in intramolecular cyclization rate, cargo release occurs notably faster with the presence of both stimuli. According to this finding, several AND logic probes have been developed that respond to a broad scope of stimuli and show remarkably improved signal-to-background contrast compared to those of monoresponsive probes. In addition, an AND logic probe that is responsive to monoamine oxidase (MAO) and leucine aminopeptidase (LAP) has been constructed for hepatopathy diagnosis. It works efficiently in living cells and mouse models. Of note, this probe can successfully differentiate cirrhotic from hepatitis B by testing the blood samples from patients.

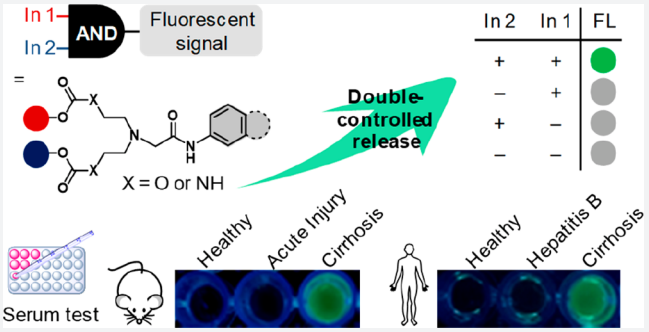

INTRODUCTION

Diseases are complex; therefore, methods for diagnosis and treatment need to achieve accurate targeting in large populations of similar diseases.[1] The development of disease is always accompanied by abnormal levels of biomolecules that can be used as biomarkers to differentiate diseased tissues and normal tissues.[2] To enhance targeting accuracy, triggering moieties have been introduced into smart materials to recognize disease-associated stimuli (e.g., pH, redox state, and enzymes),[3−5] but a single biomarker is rarely sufficient to identify a specific disease.[6−10] For example, most liver disorders share elevated transaminase levels in serum.[11] As a result, single-triggered strategies have difficulties in the accurate recognition of diseases. A multienzymatic trigger has been established to allow tumor-selective activation of the prodrug.[12] However, this multienzymatic trigger follows "OR" logic and can be activated by either stimulus. Inspired by the double-targeting strategy that achieves tumor-selective drug release,[13,14] we seek to develop an "AND" molecular logic trigger that works when both disease-associated stimuli exist, which would help to enhance diagnostic and therapeutic accuracy.

Molecular AND logic controlled release systems have been emerging as a useful platform for enhanced selectivity of cargo release.[15,16] There are three established models: dual functionalization, sequential activation, and parallel activation (Figure 1A). The dual functionalization strategy relies on two different triggering moieties anchoring two active sites in cargo molecules. This limits the diversity of the cargo backbone, and only studies about fluorescent probes have been reported with this strategy.[17−21] To overcome this limitation, the activation of two triggers functionalized at a single active site has been developed: sequential activation[22−25] and parallel activation.[26,27] However, sequential activation involves two different triggering moieties connected in series, which restricts their scope to specific triggering moieties. By contrast, systems activated by two independent reactions (parallel activation) have been proved to be generally applicable. However, it is worth noting that these polymer-based systems sterically block the function of cargo molecule, and the client drugs can be released after material degradation with a "tail" remaining, limiting further applications for developing fluorogenic probes. A generally applicable AND molecular logic trigger for the double-controlled release of intact cargo molecules is needed.[28]

Of interest, *N*,*N*-bis(2-hydroxyethyl)glycine amide, denoted as bicine amide, undergoes a rapid cleavage reaction ($t_{1/2}$ = 3 h) under aqueous conditions.[29] As shown in Figure 1B, both hydroxyl groups are involved in the cleavage process; the reaction rate is remarkably faster than that of a single hydroxyl group. Inspired by the above fact, we design a novel AND

Received: April 3, 2022
Published: June 6, 2022

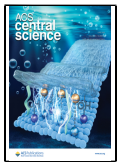

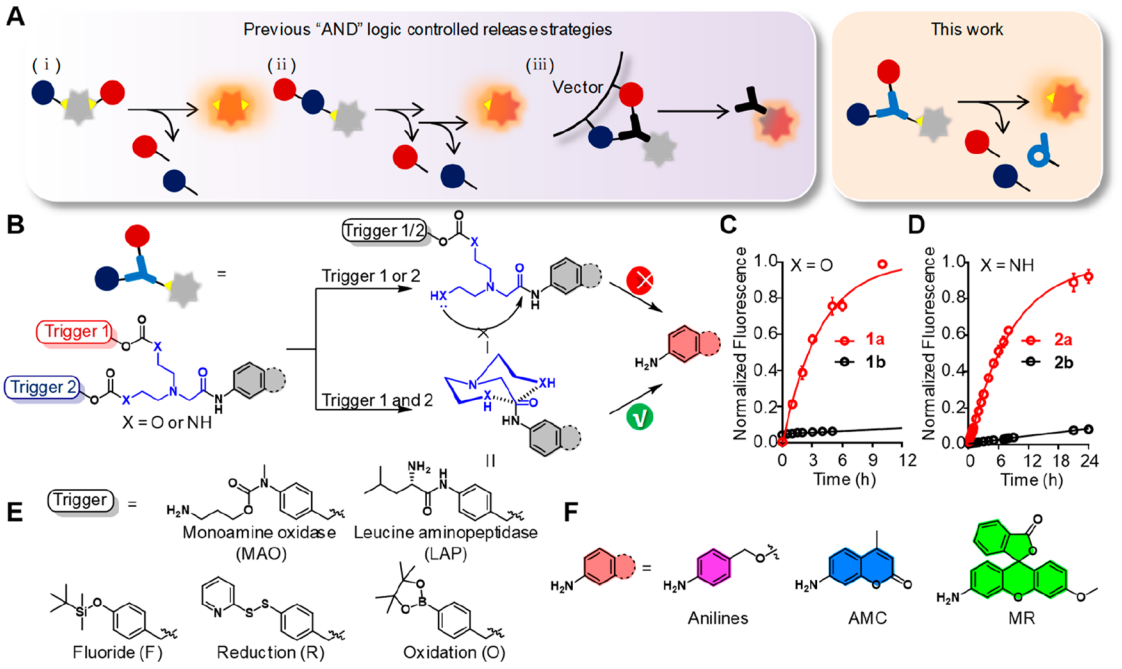

Figure 1. A generally applicable AND molecular logic gate for double-controlled release of intact functional molecules. (A) Schematic representation of previous AND logic controlled release strategies and this work. (B) This AND logic trigger functions via a unique cyclization and works if both caging groups have been removed. Kinetic curve of compounds **1a** and **1b** (C) and compounds **2a** and **2b** (D) incubated in PBS (pH = 7.4, 0.1% DMSO) (n = 3). (E) Chemical structures of representative responsive triggering moieties. (F) Chemical structures of functional cargos.

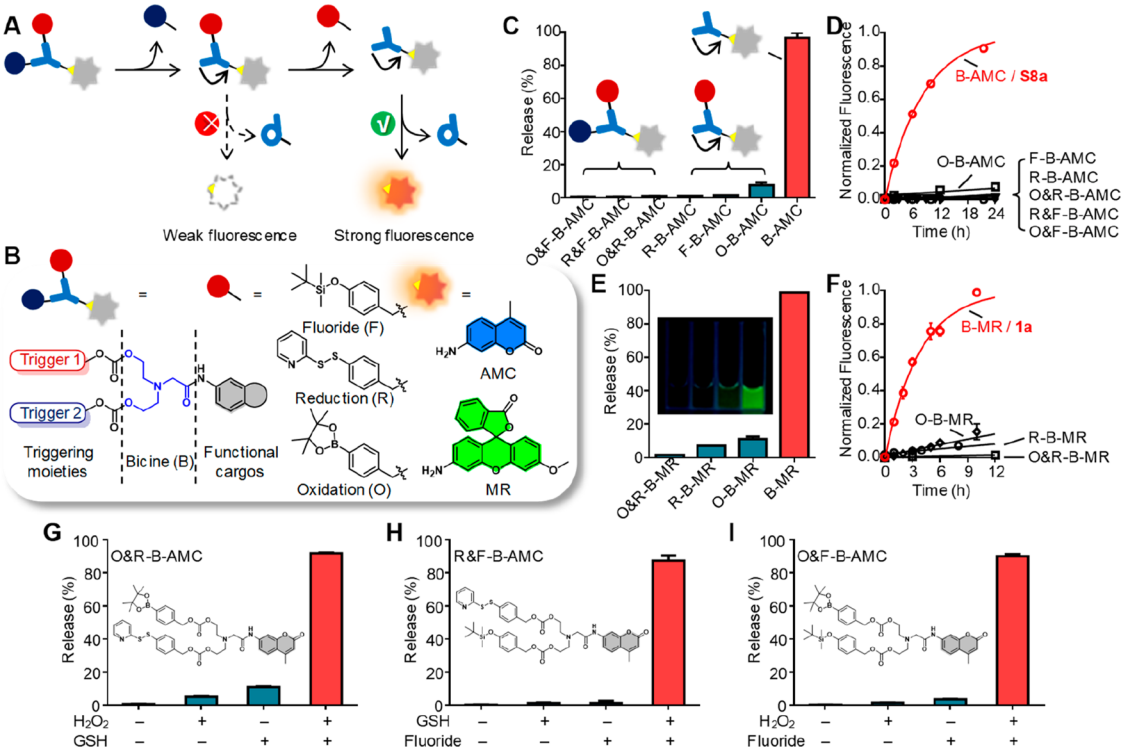

Figure 2. Bicine is identified as an AND molecular logic trigger. (A) Function mechanism of the AND molecular logic gate. (B) General design and chemical structure of the bicine-based AND logic trigger and the representative triggering moieties (F = fluoride-responsive, R = reduction-responsive, O = oxidation-responsive) and functional cargos. (C) Evaluation of AMC fluorophore release from B-AMC, O-B-AMC, F-B-AMC, R-B-AMC, O&R-B-AMC, R&F-B-AMC, and O&F-B-AMC (10 μM) incubated in PBS (pH = 7.4, 0.1% EtOH) at 24 h (n = 3). (D) Kinetic curve of AMC release in PBS (pH = 7.4, 0.1% EtOH) (n = 3). (E) Photographs (inset) and evaluation of MR release from B-MR, O-B-MR, R-B-MR, and O&R-B-MR (10 μM) incubated in PBS (pH = 7.4, 0.1% EtOH) at 10 h (n = 3). (F) Kinetic curve of MR release in PBS (pH = 7.4, 0.1% EtOH, n = 3). (G–I) Evaluation of AMC release from O&R-B-AMC, R&F-B-AMC, and O&F-B-AMC (10 μM in PBS, pH = 7.4, 0.1% EtOH) at 24 h under different stimuli (fluoride, 100 mM KF; H_2O_2, 6 mM H_2O_2; GSH, 12 mM GSH; n = 3). The above assays were performed at 37 °C without further modification.

https://doi.org/10.1021/acscentsci.2c00387
ACS Cent. Sci. 2022, 8, 837−844

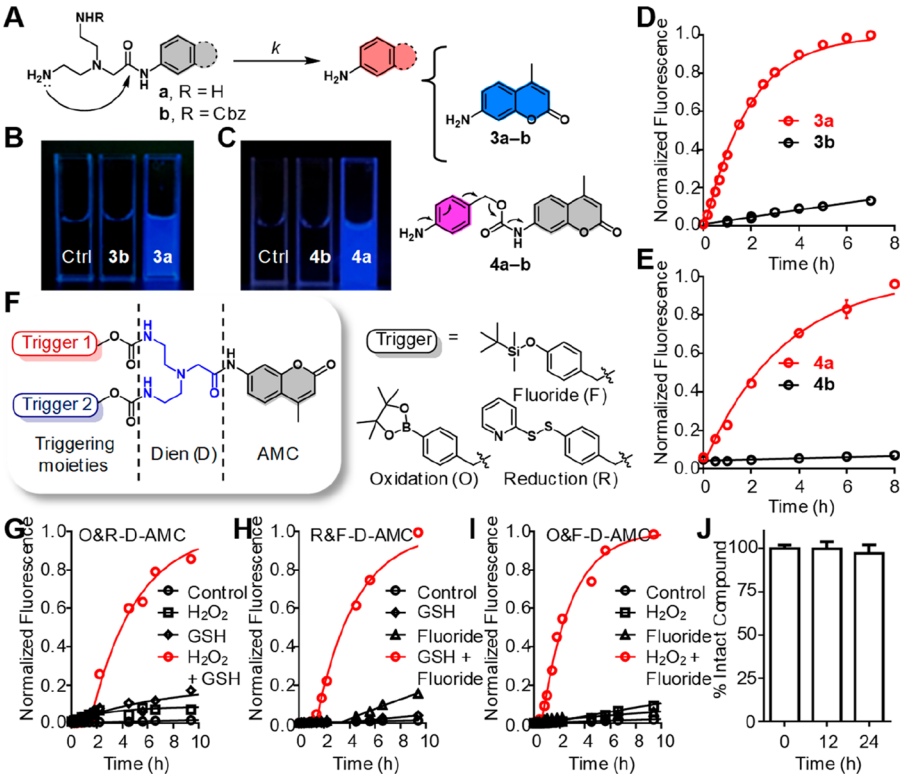

Figure 3. Dien is identified as another AND molecular logic trigger with enhanced biostability. (A) Schematic representation of the activation of a dien-based AND logic trigger. Photographs of fluorescence of compounds **3a** and **3b** (B) and **4a** and **4b** (C) (10 μM) incubated in PBS (pH = 7.4, 0.1% DMSO) at 2 h. Kinetics curve of compounds **3a** and **3b** (D) and **4a** and **4b** (E) (10 μM) incubated in PBS (pH = 7.4, 0.1% DMSO) (n = 3). (F) General design and chemical structure of the dien-based AND logic trigger. (G–I) Kinetic curve of AMC fluorescence release from O&R-D-AMC, R&F-D-AMC, and O&F-D-AMC (10 μM in PBS, pH = 7.4, 0.1% EtOH) under different stimuli (control, no treatment; fluoride, 100 mM KF; H_2O_2, 6 mM H_2O_2; GSH, 12 mM GSH; n = 3). (J) Stability of O&R-D-AMC (10 μM) incubated in DMEM with 10% FBS (n = 3). The above assays were performed at 37 °C without further modification.

molecular logic gate that would take intramolecular cyclization to release intact functional cargos when both triggering moieties have been removed (Figure 1B). By introducing the protecting groups, compounds **1b** and **2b** were synthesized to study the kinetic difference with their analogues without protection (compounds **1a** and **2a**, structure details in Scheme S1). As shown in Figure 1C,D, compounds **1a** and **2a** exhibit a fast release of 3-*O*-methyl-rhodol (MR) with half-lives of 2.60 ± 0.23 and 5.97 ± 0.21 h, respectively, which correspond to rate increases of 92.3-fold and 32.3-fold relative to compounds **1b** and **2b**. This AND molecular logic gate can be readily extendable to different triggering moieties and functional cargos (Figure 1E,F).

RESULTS AND DISCUSSION

As shown in Figure S1, carbamate (compounds **S1a** and **S1b**), amide (compounds **1a** and **1b** and compounds **S4**–**S8**), and esters (compounds **S2** and **S3**) have been screened for developing an efficient AND logic gate. It is found that compounds **S1a** and **S1b** undergo slow hydrolysis, while more electrophilic esters **S2** and **S3** hydrolyzed rapidly within 1 min. To our satisfaction, cleavage reactions of amides (compounds **1a** and **S4a**–**S8a** except for strong electron-withdrawing compound **S6**) are significantly faster than those of their single hydroxyl analogues and may function as an AND gate for biological applications. ^{1}H NMR spectroscopy is used to monitor the progress of the cleavage reaction. As shown in Figure S2, the generation of six-membered cyclic products and the corresponding ring-opening product is observed, suggesting an intramolecular cyclization mechanism.

We then wondered whether bicine phenylamides could be developed as a useful AND logic controlled release system, which can effectively release functional cargos when both stimuli are present (Figure 2A). To pursue this idea, we first introduced triggering moieties responsive to fluoride (F), reduction (R), and oxidation (O) to "bicine-caged" 7-amino-4-methylcoumarin (B-AMC/**S8a**) to form three monoprotected compounds (F-B-AMC, R-B-AMC, and O-B-AMC) and three diprotected compounds (O&R-B-AMC, R&F-B-AMC, and O&F-B-AMC; Figure 2B). Then, we compared the AMC release of these compounds with B-AMC. All compounds are dissolved in PBS (pH = 7.4, 0.1% EtOH as a cosolvent) at a final concentration of 10 μM. As shown in Figure 2C, about a 97% release of AMC is detected from B-AMC after 24 h of incubation, and that of other compounds remains below 8%. The kinetics of AMC release is further monitored by a fluorescence spectrophotometer. Both monoprotected and diprotected compounds are stable in PBS with half-lives of more than 300 h; nonetheless, the half-life is shortened to 5.82 ± 0.39 h for B-AMC (Figure 2D). The replacement of AMC with MR shows a similar fluorophore release performance. As shown in Figure 2E, strong green fluorescence is observed from bicine-caged MR (B-MR/**1a**) while almost no fluorescence increase is detected from R-B-MR, O-B-MR, or O&R-B-MR. More quantitatively, about 98% of MR is released from B-MR with a half-life of 2.60 ± 0.23 h, and this value is

https://doi.org/10.1021/acscentsci.2c00387
ACS Cent. Sci. 2022, 8, 837–844

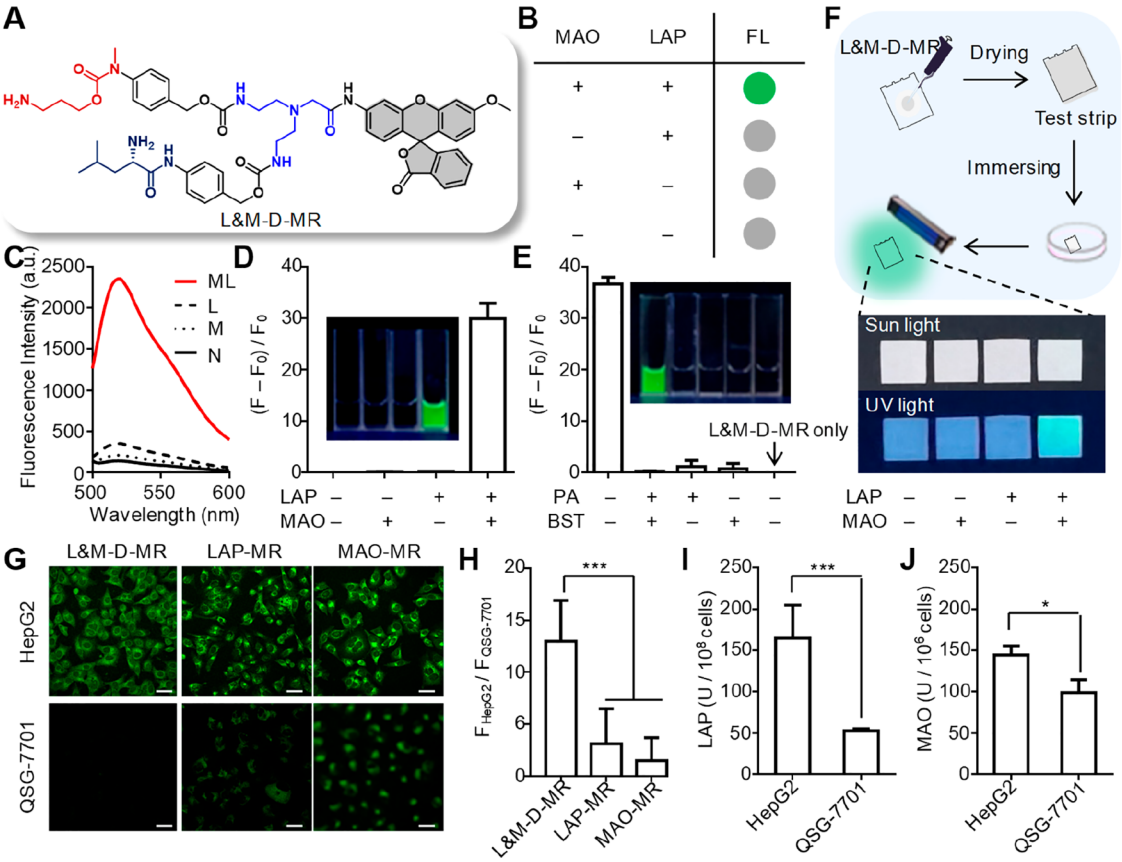

Figure 4. AND logic probe (L&M-D-MR) operated by leucine aminopeptidase (LAP) and monoamine oxidase (MAO) and its application in living cells. (A) Chemical structure of L&M-D-MR. (B) Fluorescence release of L&M-D-MR when treated by indicated stimuli. (C) Fluorescence spectra of L&M-D-MR (10 μM) under different stimuli (N indicates no treatment, M is 12.5 U/L MAO, L is 12.5 U/L LAP) in PBS (pH = 7.4, 0.1% DMSO). (D) Photographs (inset) and fluorescence response $(F - F_0)/F_0$ of L&M-D-MR (10 μM in PBS, pH = 7.4, 0.1% DMSO) in different reaction systems at 5 h (LAP, 12.5 U/L; MAO, 12.5 U/L) (n = 3). (E) Photographs (inset) and fluorescence response $(F - F_0)/F_0$ of L&M-D-MR (10 μM in PBS, pH = 7.4, 0.1% DMSO) incubated with different inhibitors at 24 h (LAP, 12.5 U/L; MAO, 12.5 U/L; PA, 100 μM; BST, 100 μM) (n = 3). (F) Preparation of test strips and photographs of test strips after the reaction with LAP (12.5 U/L) or MAO (12.5 U/L) in PBS (pH = 7.4). (G) Confocal fluorescence images of HepG2 and QSG-7701 cells incubated with L&M-D-MR, LAP-MR, or MAO-MR (10 μM in DMEM with 10% FBS) for 10 h. Scale bar, 50 μm. (H) Quantification of the cellular fluorescence intensities in panel G. Twenty fields of view were randomly chosen for each experiment (two-tailed unpaired Student's t test, ***P < 0.001). LAP activity (I) and MAO activity (J) in HepG2 and QSG-7701 cells (n = 3). A two-tailed unpaired Student's t test was performed, *P < 0.1, ***P < 0.001. The above assays were performed at 37 °C without further modification.

8−65-fold larger than that of other molecules (Figure 2F). These results suggest that the high reactivity of oxygen atoms in the bicine backbone can be efficiently silenced by the triggering moiety.

Encouraged by the above results, we attempted to evaluate the release behavior of O&R-B-AMC, R&F-B-AMC, and O&F-B-AMC under different stimuli. As shown in Figure 2G−I and Figures S3−S5, a notably faster release of AMC occurs when both programmed stimuli were present. Given the initial success of the bicine series, we hope to be able to replace the selected triggering moieties with other chemically orthogonal moieties responsive to pH,[4,5] light,[30−32] radiation,[33,34] or chemical triggers.[13,35−40] Therefore, bicine was identified as a generalized structure of AND molecular logic triggers.

To examine whether this bicine-based AND logic controlled release system works in living cells, we chose O&R-B-AMC as a model compound and conducted a stability study in cell culture medium. Unfortunately, less than 5% of O&R-B-AMC remains after a 24 h incubation in DMEM with 10% FBS, although it is stable in PBS (Figure S6). We attributed the instability to carbonate linkage. To address this problem, we attempted to replace oxygen in nucleophilic sites with nitrogen resulting in a more stable carbamate linkage, and the resulting diethylenetriamine-*N*-phenylacetamide was denoted as dien.

To develop an alternative AND logic trigger with enhanced stability, we prepared a series of "dien-caged" fluorophores (compounds **3a** and **4a**) and the related monoprotected compounds **3b** and **4b** (Figure 3A, structures details in Scheme S6) to evaluate the kinetic profiles of the cleavage reaction with dien. As shown in Figure 3B,C, strong fluorescence is observed from compounds **3a** and **4a** while almost no fluorescence increase is detected from compounds **3b** and **4b**. The kinetics of fluorophore release is further monitored by a fluorescence spectrophotometer (Figure 3D,E). Fluorescence signals of compounds **3a** and **4a** grow with time and reach the plateau in about 7 and 12 h, respectively. Compounds **3a** and **4a** exhibit a rapid release of fluorophores with half-lives of 1.29 ± 0.05 and 2.31 ± 0.19 h, respectively, which correspond to rate increases of 26.8-fold and 95.8-fold as compared to those of compounds **3b** and **4b**. Therefore, we concluded that dien undergoes faster intramolecular cyclization to release free anilines than single aminoethyl analogues.

https://doi.org/10.1021/acscentsci.2c00387
ACS Cent. Sci. 2022, 8, 837−844

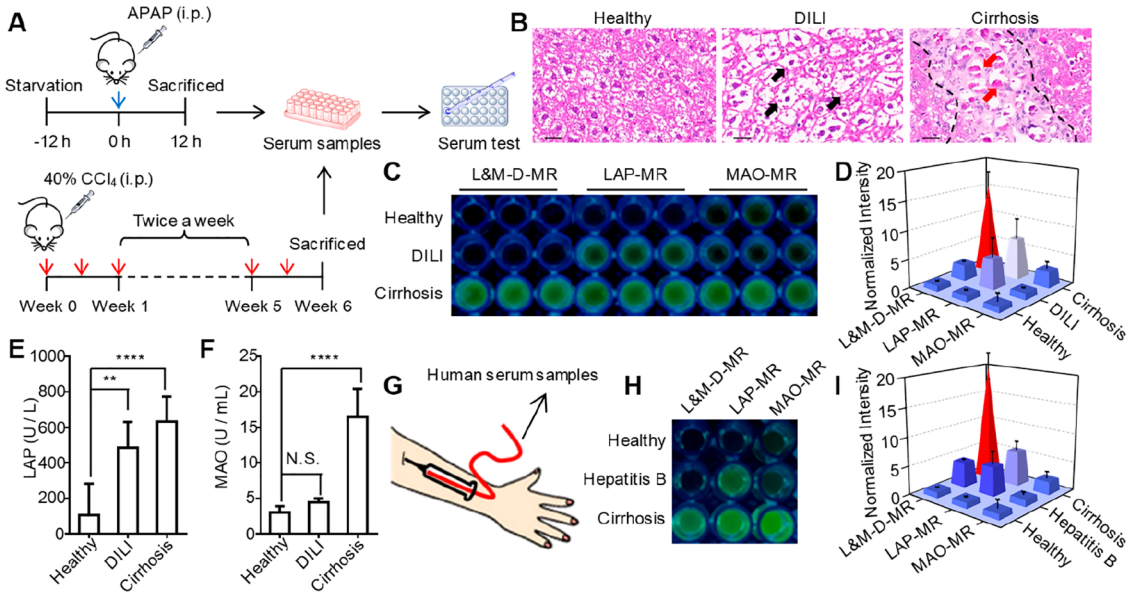

Figure 5. Serum testing with the AND logic probe can accurately and effectively differentiate liver cirrhosis from hepatitis in patients. (A) Schematic representation of constructing acetaminophen (APAP) induced liver injury (DILI) models and tetrachloromethane (CCl_4) induced liver cirrhosis models in Kunming (KM) mice. (B) H&E staining images of the liver tissues in healthy, DILI, and cirrhotic mice. Black arrows, ballooning degeneration; red arrows, necrotic hepatocytes; and black dashed line, fibrotic bands. Scale bar, 25 μm. (C) Photographs of mouse serum samples treated with L&M-D-MR, LAP-MR, or MAO-MR (50 μM in PBS, pH = 7.4, 0.5% DMSO) in 96-well plates at 37 °C. (D) Quantification of the fluorescence intensities in panel C. (E, F) LAP and MAO level in the serum of healthy, DILI, and cirrhotic mice (n = 5). A two-tailed unpaired Student's t test was performed; N.S., no significant difference, $^{**}P < 0.01$, $^{****}P < 0.0001$. (G) Diagram of human serum collection. (H) Photographs of human serum samples treated with L&M-D-MR, LAP-MR, or MAO-MR (50 μM in PBS, pH = 7.4, 0.5% DMSO) in 96-well plates at 37 °C. (I) Quantification of the fluorescence intensities in Figure S19.

Encouraged by the above results, we sought to evaluate the release behavior of the dien series under different stimuli. Thus, we introduced three different triggering moieties (F = fluoride-responsive, R = reduction-responsive, and O = oxidation-responsive) to dien-caged AMC (D-AMC/**3a**) to form three diprotected compounds (O&R-D-AMC, O&F-D-AMC, and R&F-D-AMC) (Figure 3F). As shown in Figure 3G−I, all three compounds achieve a complete release of AMC in the presence of both stimuli within 10 h. Moreover, the release behavior is unaffected by different addition orders of the two stimuli (Figure S7). Given the initial success of the dien series, we chose O&R-D-AMC as a model compound and tested its stability in cell culture medium. To our satisfaction, O&R-D-AMC shows high stability in DMEM with 10% FBS where more than 95% of O&R-D-AMC remains after 24 h of incubation (Figure 3J). Taken together, dien is another AND molecular logic trigger with enhanced biostability.

To examine whether a dien-based AND logic controlled release system works in living cells, we prepared a dien-based AND logic probe, denoted as L&M-D-MR, which contains a monoamine oxidase (MAO)-responsive moiety and leucine aminopeptidase (LAP)-responsive moiety (Figure 4A). Then, we examined the kinetic performance of L&M-D-MR in PBS (pH = 7.4, 0.1% DMSO as a cosolvent) under different combinations of enzymes using a fluorescence spectrophotometer and UV−vis spectrophotometer (Figure 4B−F and Figure S8). As shown in Figure 4C and Figure S8A, when both enzymes are presented, a significant increase in the fluorescence emission at 520 nm and a remarkable red shift of the absorption can be observed. More quantitatively, the fluorescence response $(F - F_0)/F_0$ of L&M-D-MR incubated with both MAO and LAP is 200 times higher than those in other treatments within 5 h (Figure 4D). Then, we monitored the MR release of L&M-D-MR over a longer period. As shown in Figure S8B,C, a reaction with both MAO (12.5 U/L) and LAP (12.5 U/L) induces a gradual increase of fluorescence, reaching a plateau in about 24 h, while either enzyme only leads to a slight fluorescence increase. In addition, the increase in the fluorescence signal at 520 nm depends on the concentrations of LAP and MAO in a linear manner (Figure S8D,E), and the detection limits of MAO and LAP are calculated to be 0.249 and 0.877 U/L, respectively (Figure S8F). After validating the kinetic performance of L&M-D-MR, we carried out an enzyme inhibition assay to confirm the specificity of L&M-D-MR's response. As illustrated in Figure 4E, 100 μM PA (MAO inhibitor) and 100 μM BST (LAP inhibitor) decrease the fluorescence signal by 163 times compared with the control group without an inhibitor. As expected, it shows background fluorescence in the presence of either inhibitor, proving the specificity of L&M-D-MR toward MAO and LAP. Encouraged by the above results, we expanded the scope of applications of the AND logic probe to the test strip. Figure 4F shows the preparation and usage of test strips containing L&M-D-MR. Pleasingly, stronger green fluorescence is observed in the test strip treated with both LAP and MAO under 365 nm UV light. Taken together, we successfully constructed an AND logic probe responsive to two different enzymes simultaneously.

For further applications in living cells or animals, the stability assay and reactivity study in both DMEM (with 10% FBS) and 100-fold diluted serum were performed by UPLC−MS analysis. As expected, L&M-D-MR shows excellent biostability in both cell culture medium and 100-fold diluted serum (Figure S9). As shown in Figure S10, when treated with either LAP or MAO, a new peak can be observed, referring to M-D-MR or L-D-MR by mass analysis, and only slight degradation

https://doi.org/10.1021/acscentsci.2c00387
ACS Cent. Sci. 2022, 8, 837−844

occurs within 12 h. In contrast, when L&M-D-MR is treated with both enzymes, a new peak at 0.93 min is observed, referring to D-MR, and a shift toward longer retention time is detected after 12 h, which is due to much faster intramolecular cyclization than M-D-MR and L-D-MR. Therefore, we would suggest that the enzyme-triggered activation of the AND logic probe would not be affected by adding serum.

Next, we examined the imaging performance of L&M-D-MR in liver cancer cells (HepG2) and normal liver cells (QSG-7701). For comparison, we prepared two reference probes MAO-MR and LAP-MR, which only respond to MAO and LAP, respectively (Figures S11 and S12). As shown in Figure S13, no significant cytotoxicities of L&M-D-MR, MAO-MR, and LAP-MR are observed in both cell lines within 12 h, suggesting good biocompatibility. Then, we incubated HepG2 cells, which overexpress both MAO and LAP, with 10 μM L&M-D-MR in DMEM for confocal imaging. Notably, treating HepG2 cells with L&M-D-MR renders the appearance of strong green fluorescence (Figure S14A). By contrast, HepG2 cells pretreated with 100 μM PA and/or 100 μM BST retain background fluorescence. As shown in Figure S14B, the fluorescence intensity of cells treated with L&M-D-MR is a 5.88-fold increase compared with cells pretreated with inhibitors. In addition, the fluorescence signal of MAO-MR and LAP-MR in HepG2 cells can also be decreased by inhibitors (Figure S15). These results indicate that the response of three probes in HepG2 cells is determined by enzymatic activation. Next, we treated QSG-7701 cells, which only show high MAO activity (Figure 4I,J), with these three probes. Interestingly, L&M-D-MR exhibits a higher ratio of F_{HepG2} to $F_{QSG\text{-}7701}$ (up to 13.0) compared with MAO-MR and LAP-MR, which correspond to 3.11 ± 3.37 and 1.49 ± 2.22, respectively (Figure 4G,H). The presented fluorescence differences are relative to enzyme activity differences among cells, suggesting that this AND logic probe has a potential application in the identification of specific cell lines.

To further explore the potential of this dien-based AND logic controlled release system for biomedical applications, we turned to hepatopathy differentiation because both LAP and MAO are key markers of liver function tests.[25] LAP is an important enzyme that preferentially breaks down the amide bond between leucine residues and the N-terminus of peptides and proteins.[41,42] Elevated serum levels of LAP have been found in many liver disorders, such as liver hepatitis, liver cirrhosis, and liver carcinoma.[11,43,44] MAO is a kind of flavoenzyme that is involved in the oxidation of monoamine.[45,46] The level of serum MAO activity increases significantly in early stage fibrosis, making it an important marker for the early diagnosis of cirrhosis.[47,48] Although some MAO-responsive and LAP-responsive probes have been reported,[49] their nonspecific signal in tissues with low enzyme activity may limit further biomedical applications. As illustrated in Figure 4B, a stronger fluorescence signal occurs in the presence of both enzymes compared to either enzyme, and this pattern endows the AND logic probe with high selectivity. Thus, we attempted to explore the potential of a dien-based AND logic controlled release system for accurate hepatopathy differentiation.

As shown in Figure 5A, Kunming (KM) mice are divided into two groups, one of which is intraperitoneally injected with acetaminophen (APAP) to induce liver injury (DILI). The other group is intraperitoneally injected with tetrachloromethane (CCl_4) to build the cirrhotic model. Then, all of the mice are sacrificed, and blood and liver tissues are harvested. As illustrated in Figure 5B and Figure S16, ballooning degeneration of the hepatocytes (black arrows) is found in the DILI model while clearly fibrotic bands (black dashed line) and necrotic hepatocytes (red arrows) can be observed in the cirrhotic mode indicating the successful construction of both mice models. Then, we incubated different serum samples with 50 μM L&M-D-MR, LAP-MR, and MAO-MR in 96-well plates at 37 °C. As shown in Figure 5C and Figure S17, all three probes exhibit a strong green fluorescence signal in the serum of cirrhotic mice. However, increased fluorescence is also observed in the serum of DILI mice treated with LAP-MR, and serums from both healthy mice and DILI mice are lighted by MAO-MR. To confirm the reliability of our results, we measured the serum level of LAP and MAO using commercial kits. As expected, the serum level of LAP increases significantly in both DILI mice and cirrhotic mice, corresponding to a 4.62-fold and 5.99-fold change over healthy mice, respectively (Figure 5E). Although there is a 5.46-fold increase in the serum level of MAO in cirrhotic mice, the background activity of MAO in healthy mice and DILI mice could not be neglected (more than 3000 U/L) (Figure 5F). Therefore, using LAP-MR, it is hard to distinguish cirrhotic mice from DILI mice due to the elevated level of LAP in both models. It is also difficult for MAO-MR to distinguish cirrhotic mice from DILI mice and healthy mice because of the background activity of MAO in both mice. On the contrary, L&M-D-MR exhibits an excellent performance for distinguishing cirrhotic mice from DILI mice and healthy mice with a high signal-to-background ratio of 15.7 (Figure 5D).

These encouraging results prompt us to apply L&M-D-MR for identifying different hepatopathies by human serum testing (Figure 5G). As shown in Figure S18, the serum levels of both LAP and MAO increase in cirrhotic patients compared to healthy people (6.51 times and 4.20 times enhancement, respectively) while only an elevated serum level of LAP is observed in hepatitis B patients. Then, we incubated human serum samples with L&M-D-MR, LAP-MR, and MAO-MR under the same condition used in mouse serum testing. To our satisfaction, L&M-D-MR shows a much stronger green fluorescence signal in the serum of cirrhotic patients with a high signal-to-background ratio of 20.3 (Figure 5H,I and Figure S19). These data indicate that L&M-D-MR can accurately distinguish cirrhotic patients from healthy people and hepatitis B patients by serum testing. On the other hand, LAP-MR cannot differentiate cirrhotic patients from hepatitis B patients, and MAO-MR is challenged by a high background signal. Though LAP-MR alone may distinguish hepatitis B patients from healthy patients, this single-activated probe exhibits notably less contrast that may result in a false-positive diagnosis. As a certain level of LAP can be found in the serum of healthy people (77.80 ± 57.39 U/L, Figure S18), it can trigger the activation of LAP-MR but not the AND-logic gated probe. As shown in Figure 5H and Figure S19, the single-activated probe exhibits a notably higher background signal (LAP-MR, 248.50) than the AND-gated probe (L&M-D-MR, 92.58). Taken together, we attributed the diagnostic accuracy of L&M-D-MR to its AND logic release pattern, and it holds a promising future in hepatopathy diagnosis in the clinic.

In conclusion, we have introduced a novel modular design of an AND molecular logic trigger responsive to two disease-associated stimuli simultaneously. Building upon this discovery, a novel AND logic controlled release system was

https://doi.org/10.1021/acscentsci.2c00387
ACS Cent. Sci. 2022, 8, 837−844

developed with enhanced selectivity and was successfully applied to hepatopathy differentiation in patients. This system can be readily extended to covalently tether other triggering moieties to drug molecules, proteins, and nucleic acids, affording accurate diagnosis and therapy.

■ ASSOCIATED CONTENT

Supporting Information

The Supporting Information is available free of charge at https://pubs.acs.org/doi/10.1021/acscentsci.2c00387.

Reagents and apparatus, chemical synthetic methods, experimental details, supplementary figures, and NMR spectra and high-resolution mass spectra for all compounds (PDF)

Transparent Peer Review report available (PDF)

■ AUTHOR INFORMATION

Corresponding Author

Zhibo Liu − *Beijing National Laboratory for Molecular Sciences, Radiochemistry and Radiation Chemistry Key Laboratory of Fundamental Science, NMPA Key Laboratory for Research and Evaluation of Radiopharmaceuticals, Key Laboratory of Bioorganic Chemistry and Molecular Engineering of Ministry of Education, College of Chemistry and Molecular Engineering and Peking University−Tsinghua University Center for Life Sciences, Peking University, Beijing 100871, China;* orcid.org/0000-0002-5587-4165; Email: zbliu@pku.edu.cn

Authors

Mengqi Chen − *Beijing National Laboratory for Molecular Sciences, Radiochemistry and Radiation Chemistry Key Laboratory of Fundamental Science, NMPA Key Laboratory for Research and Evaluation of Radiopharmaceuticals, Key Laboratory of Bioorganic Chemistry and Molecular Engineering of Ministry of Education, College of Chemistry and Molecular Engineering, Peking University, Beijing 100871, China*

Chunhong Wang − *Beijing National Laboratory for Molecular Sciences, Radiochemistry and Radiation Chemistry Key Laboratory of Fundamental Science, NMPA Key Laboratory for Research and Evaluation of Radiopharmaceuticals, Key Laboratory of Bioorganic Chemistry and Molecular Engineering of Ministry of Education, College of Chemistry and Molecular Engineering, Peking University, Beijing 100871, China*

Zexuan Ding − *Beijing National Laboratory for Molecular Sciences, Radiochemistry and Radiation Chemistry Key Laboratory of Fundamental Science, NMPA Key Laboratory for Research and Evaluation of Radiopharmaceuticals, Key Laboratory of Bioorganic Chemistry and Molecular Engineering of Ministry of Education, College of Chemistry and Molecular Engineering, Peking University, Beijing 100871, China*

Hao Wang − *Department of Radiation Oncology, Peking University Third Hospital, Beijing 100191, China*

Yu Wang − *Department of Neurosurgery, Peking Union Medical College Hospital, Chinese Academy of Medical Sciences and Peking Union Medical College, Beijing 100730, China*

Complete contact information is available at: https://pubs.acs.org/10.1021/acscentsci.2c00387

Notes

The authors declare no competing financial interest.

■ ACKNOWLEDGMENTS

This work was funded by the Beijing Municipal Natural Science Foundation (Grant Z200018), the National Nature Science Foundation of China (Grant U1867209), the Ministry of Science and Technology of the People's Republic of China (Grants 2021YFA1601400 and 2017YFA0506300), the Special Foundation of Beijing Municipal Education Commission (Grant 3500-12020123), and Li Ge-Zhao Ning Life Science Youth Research Foundation (LGZNQN202004) to Z.L. We are thankful for the facility support from the Analytical Instrumentation Center of Peking University. We thank Prof. Huimin Ma for providing HepG2 cell lines. We also thank Dr. Hao Wang and Dr. Jingjin Liang for providing human blood samples. We thank Mr. Xuanyu Wang for his contribution in chemical synthesis.

■ REFERENCES

(1) Tregubov, A. A.; Nikitin, P. I.; Nikitin, M. P. Advanced Smart Nanomaterials with Integrated Logic-Gating and Biocomputing: Dawn of Theranostic Nanorobots. *Chem. Rev.* **2018**, *118* (20), 10294−10348.

(2) Broza, Y. Y.; Zhou, X.; Yuan, M.; Qu, D.; Zheng, Y.; Vishinkin, R.; Khatib, M.; Wu, W.; Haick, H. Disease Detection with Molecular Biomarkers: From Chemistry of Body Fluids to Nature-Inspired Chemical Sensors. *Chem. Rev.* **2019**, *119* (22), 11761−11817.

(3) Dai, Y.; Xu, C.; Sun, X.; Chen, X. Nanoparticle design strategies for enhanced anticancer therapy by exploiting the tumour microenvironment. *Chem. Soc. Rev.* **2017**, *46* (12), 3830−3852.

(4) Blum, A. P.; Kammeyer, J. K.; Rush, A. M.; Callmann, C. E.; Hahn, M. E.; Gianneschi, N. C. Stimuli-responsive nanomaterials for biomedical applications. *J. Am. Chem. Soc.* **2015**, *137* (6), 2140−2154.

(5) Mura, S.; Nicolas, J.; Couvreur, P. Stimuli-responsive nanocarriers for drug delivery. *Nat. Mater.* **2013**, *12* (11), 991−1003.

(6) Nikitin, M. P.; Shipunova, V. O.; Deyev, S. M.; Nikitin, P. I. Biocomputing based on particle disassembly. *Nat. Nanotechnol.* **2014**, *9* (9), 716−722.

(7) Hou, B.; Zhou, L.; Wang, H.; Saeed, M.; Wang, D.; Xu, Z.; Li, Y.; Yu, H. Engineering Stimuli-Activatable Boolean Logic Prodrug Nanoparticles for Combination Cancer Immunotherapy. *Adv. Mater.* **2020**, *32* (12), 1907210−1907221.

(8) Wang, D.; Li, S.; Zhao, Z.; Zhang, X.; Tan, W. Engineering a Second-Order DNA Logic-Gated Nanorobot to Sense and Release on Live Cell Membranes for Multiplexed Diagnosis and Synergistic Therapy. *Angew. Chem., Int. Ed.* **2021**, *60* (29), 15816−15820.

(9) Dai, X. X.; Han, K.; Ma, Z. Y.; Han, H. Y. A Chimeric Peptide Logic Gate for Orthogonal Stimuli-Triggered Precise Tumor Therapy. *Adv. Funct. Mater.* **2018**, *28* (47), 1804609−1804620.

(10) Tang, L.; Yang, Z.; Zhou, Z.; Ma, Y.; Kiesewetter, D. O.; Wang, Z.; Fan, W.; Zhu, S.; Zhang, M.; Tian, R.; et al. A Logic-Gated Modular Nanovesicle Enables Programmable Drug Release for On-Demand Chemotherapy. *Theranostics* **2019**, *9* (5), 1358−1368.

(11) Huang, Y.; Qi, Y.; Zhan, C.; Zeng, F.; Wu, S. Diagnosing Drug-Induced Liver Injury by Multispectral Optoacoustic Tomography and Fluorescence Imaging Using a Leucine-Aminopeptidase-Activated Probe. *Anal. Chem.* **2019**, *91* (13), 8085−8092.

(12) Amir, R. J.; Popkov, M.; Lerner, R. A.; Barbas, C. F., 3rd; Shabat, D. Prodrug activation gated by a molecular "OR" logic trigger. *Angew. Chem., Int. Ed.* **2005**, *44* (28), 4378−4381.

(13) Wang, Q.; Wang, Y.; Ding, J.; Wang, C.; Zhou, X.; Gao, W.; Huang, H.; Shao, F.; Liu, Z. A bioorthogonal system reveals antitumour immune function of pyroptosis. *Nature* **2020**, *579* (7799), 421−426.

(14) Duan, D.; Dong, H.; Tu, Z.; Wang, C.; Fu, Q.; Chen, J.; Zhong, H.; Du, P.; Sun, L. D.; Liu, Z. Desilylation Induced by Metal Fluoride

Nanocrystals Enables Cleavage Chemistry In Vivo. *J. Am. Chem. Soc.* **2021**, *143* (5), 2250−2255.
(15) de Silva, A. P.; Uchiyama, S. Molecular logic and computing. *Nat. Nanotechnol.* **2007**, *2* (7), 399−410.
(16) Erbas-Cakmak, S.; Kolemen, S.; Sedgwick, A. C.; Gunnlaugsson, T.; James, T. D.; Yoon, J.; Akkaya, E. U. Molecular logic gates: the past, present and future. *Chem. Soc. Rev.* **2018**, *47* (7), 2228−2248.
(17) Wu, L. L.; Huang, J. G.; Pu, K. Y.; James, T. D. Dual-locked spectroscopic probes for sensing and therapy. *Nat. Rev. Chem.* **2021**, *5* (6), 406−421.
(18) Halabi, E. A.; Thiel, Z.; Trapp, N.; Pinotsi, D.; Rivera-Fuentes, P. A Photoactivatable Probe for Super-Resolution Imaging of Enzymatic Activity in Live Cells. *J. Am. Chem. Soc.* **2017**, *139* (37), 13200−13207.
(19) Thiel, Z.; Rivera-Fuentes, P. Single-Molecule Imaging of Active Mitochondrial Nitroreductases Using a Photo-Crosslinking Fluorescent Sensor. *Angew. Chem., Int. Ed.* **2019**, *58* (33), 11474−11478.
(20) Zhang, Y.; Yan, C.; Wang, C.; Guo, Z.; Liu, X.; Zhu, W. H. A Sequential Dual-Lock Strategy for Photoactivatable Chemiluminescent Probes Enabling Bright Duplex Optical Imaging. *Angew. Chem., Int. Ed.* **2020**, *59* (23), 9059−9066.
(21) Goldberg, J. M.; Wang, F.; Sessler, C. D.; Vogler, N. W.; Zhang, D. Y.; Loucks, W. H.; Tzounopoulos, T.; Lippard, S. J. Photoactivatable Sensors for Detecting Mobile Zinc. *J. Am. Chem. Soc.* **2018**, *140* (6), 2020−2023.
(22) Prost, M.; Hasserodt, J. "Double gating"–a concept for enzyme-responsive imaging probes aiming at high tissue specificity. *Chem. Commun.* **2014**, *50* (94), 14896−14899.
(23) Feng, W.; Gao, C.; Liu, W.; Ren, H.; Wang, C.; Ge, K.; Li, S.; Zhou, G.; Li, H.; Wang, S.; et al. A novel anticancer theranostic pro-prodrug based on hypoxia and photo sequential control. *Chem. Commun.* **2016**, *52* (60), 9434−9437.
(24) Bargh, J. D.; Walsh, S. J.; Ashman, N.; Isidro-Llobet, A.; Carroll, J. S.; Spring, D. R. A dual-enzyme cleavable linker for antibody-drug conjugates. *Chem. Commun.* **2021**, *57* (28), 3457−3460.
(25) Liu, Y.; Teng, L.; Xu, C.; Liu, H. W.; Xu, S.; Guo, H.; Yuan, L.; Zhang, X. B. A "Double-Locked" and enzyme-activated molecular probe for accurate bioimaging and hepatopathy differentiation. *Chem. Sci.* **2019**, *10* (47), 10931−10936.
(26) Badeau, B. A.; Comerford, M. P.; Arakawa, C. K.; Shadish, J. A.; DeForest, C. A. Engineered modular biomaterial logic gates for environmentally triggered therapeutic delivery. *Nat. Chem.* **2018**, *10* (3), 251−258.
(27) Zhang, P.; Gao, D.; An, K.; Shen, Q.; Wang, C.; Zhang, Y.; Pan, X.; Chen, X.; Lyv, Y.; Cui, C.; et al. A programmable polymer library that enables the construction of stimuli-responsive nanocarriers containing logic gates. *Nat. Chem.* **2020**, *12* (4), 381−390.
(28) Dal Corso, A.; Arosio, S.; Arrighetti, N.; Perego, P.; Belvisi, L.; Pignataro, L.; Gennari, C. A trifunctional self-immolative spacer enables drug release with two non-sequential enzymatic cleavages. *Chem. Commun.* **2021**, *57* (63), 7778−7781.
(29) Suggs, J. W.; Pires, R. M. Facile hydrolysis and formation of amide bonds by N-hydroxyethylation of α-amino acids. *Tetrahedron Lett.* **1997**, *38* (13), 2227−2230.
(30) Klan, P.; Solomek, T.; Bochet, C. G.; Blanc, A.; Givens, R.; Rubina, M.; Popik, V.; Kostikov, A.; Wirz, J. Photoremovable protecting groups in chemistry and biology: reaction mechanisms and efficacy. *Chem. Rev.* **2013**, *113* (1), 119−191.
(31) Weinstain, R.; Slanina, T.; Kand, D.; Klan, P. Visible-to-NIR-Light Activated Release: From Small Molecules to Nanomaterials. *Chem. Rev.* **2020**, *120* (24), 13135−13272.
(32) Ruskowitz, E. R.; DeForest, C. A. Photoresponsive biomaterials for targeted drug delivery and 4D cell culture. *Nat. Rev. Mater.* **2018**, *3* (2), 17087−17103.
(33) Fu, Q.; Li, H.; Duan, D.; Wang, C.; Shen, S.; Ma, H.; Liu, Z. External-Radiation-Induced Local Hydroxylation Enables Remote Release of Functional Molecules in Tumors. *Angew. Chem., Int. Ed.* **2020**, *59* (48), 21546−21552.
(34) Geng, J.; Zhang, Y.; Gao, Q.; Neumann, K.; Dong, H.; Porter, H.; Potter, M.; Ren, H.; Argyle, D.; Bradley, M. Switching on prodrugs using radiotherapy. *Nat. Chem.* **2021**, *13* (8), 805−810.
(35) Wang, C. H.; Hong, H. Y.; Chen, M. Q.; Ding, Z. X.; Rui, Y. C.; Qi, J. Y.; Li, Z. C.; Liu, Z. B. A Cationic Micelle as In Vivo Catalyst for Tumor-Localized Cleavage Chemistry. *Angew. Chem., Int. Ed.* **2021**, *60* (36), 19750−19758.
(36) Rossin, R.; Versteegen, R. M.; Wu, J.; Khasanov, A.; Wessels, H. J.; Steenbergen, E. J.; Ten Hoeve, W.; Janssen, H. M.; van Onzen, A.; Hudson, P. J.; et al. Chemically triggered drug release from an antibody-drug conjugate leads to potent antitumour activity in mice. *Nat. Commun.* **2018**, *9* (1), 1484−1494.
(37) Yao, Q.; Lin, F.; Fan, X.; Wang, Y.; Liu, Y.; Liu, Z.; Jiang, X.; Chen, P. R.; Gao, Y. Synergistic enzymatic and bioorthogonal reactions for selective prodrug activation in living systems. *Nat. Commun.* **2018**, *9* (1), 5032−5040.
(38) Wang, J.; Wang, X.; Fan, X.; Chen, P. R. Unleashing the Power of Bond Cleavage Chemistry in Living Systems. *ACS Cent. Sci.* **2021**, *7* (6), 929−943.
(39) Bruemmer, K. J.; Crossley, S. W. M.; Chang, C. J. Activity-Based Sensing: A Synthetic Methods Approach for Selective Molecular Imaging and Beyond. *Angew. Chem., Int. Ed. Engl.* **2020**, *59* (33), 13734−13762.
(40) Chan, J.; Dodani, S. C.; Chang, C. J. Reaction-based small-molecule fluorescent probes for chemoselective bioimaging. *Nat. Chem.* **2012**, *4* (12), 973−84.
(41) Zhang, W.; Liu, F.; Zhang, C.; Luo, J. G.; Luo, J.; Yu, W.; Kong, L. Near-Infrared Fluorescent Probe with Remarkable Large Stokes Shift and Favorable Water Solubility for Real-Time Tracking Leucine Aminopeptidase in Living Cells and In Vivo. *Anal. Chem.* **2017**, *89* (22), 12319−12326.
(42) Sakabe, M.; Asanuma, D.; Kamiya, M.; Iwatate, R. J.; Hanaoka, K.; Terai, T.; Nagano, T.; Urano, Y. Rational design of highly sensitive fluorescence probes for protease and glycosidase based on precisely controlled spirocyclization. *J. Am. Chem. Soc.* **2013**, *135* (1), 409−414.
(43) Wang, B.; Chen, Z.; Cen, X.; Liang, Y.; Tan, L.; Liang, E.; Zheng, L.; Zheng, Y.; Zhan, Z.; Cheng, K. A highly selective and sensitive chemiluminescent probe for leucine aminopeptidase detection in vitro, in vivo and in human liver cancer tissue. *Chem. Sci.* **2022**, *13* (8), 2324−2330.
(44) He, X.; Li, L.; Fang, Y.; Shi, W.; Li, X.; Ma, H. In vivo imaging of leucine aminopeptidase activity in drug-induced liver injury and liver cancer via a near-infrared fluorescent probe. *Chem. Sci.* **2017**, *8* (5), 3479−3483.
(45) Li, L.; Zhang, C. W.; Chen, G. Y.; Zhu, B.; Chai, C.; Xu, Q. H.; Tan, E. K.; Zhu, Q.; Lim, K. L.; Yao, S. Q. A sensitive two-photon probe to selectively detect monoamine oxidase B activity in Parkinson's disease models. *Nat. Commun.* **2014**, *5* (1), 3276−3285.
(46) Fang, H.; Zhang, H.; Li, L.; Ni, Y.; Shi, R.; Li, Z.; Yang, X.; Ma, B.; Zhang, C.; Wu, Q.; et al. Rational Design of a Two-Photon Fluorogenic Probe for Visualizing Monoamine Oxidase A Activity in Human Glioma Tissues. *Angew. Chem., Int. Ed.* **2020**, *59* (19), 7536−7541.
(47) Fan, N.; Wu, C.; Zhou, Y.; Wang, X.; Li, P.; Liu, Z.; Tang, B. Rapid Two-Photon Fluorescence Imaging of Monoamine Oxidase B for Diagnosis of Early-Stage Liver Fibrosis in Mice. *Anal. Chem.* **2021**, *93* (18), 7110−7117.
(48) Kyritsi, K.; Chen, L.; O'Brien, A.; Francis, H.; Hein, T. W.; Venter, J.; Wu, N.; Ceci, L.; Zhou, T.; Zawieja, D.; et al. Modulation of the Tryptophan Hydroxylase 1/ Monoamine Oxidase-A/ 5-Hydroxytryptamine/ 5-Hydroxytryptamine Receptor 2A/2B/2C Axis Regulates Biliary Proliferation and Liver Fibrosis During Cholestasis. *Hepatology* **2020**, *71* (3), 990−1008.
(49) Liu, H. W.; Chen, L.; Xu, C.; Li, Z.; Zhang, H.; Zhang, X. B.; Tan, W. Recent progresses in small-molecule enzymatic fluorescent probes for cancer imaging. *Chem. Soc. Rev.* **2018**, *47* (18), 7140−7180.

https://doi.org/10.1021/acscentsci.2c00387
ACS Cent. Sci. 2022, 8, 837−844